Supplementary Information

Evaluation of Dynamical Downscaling for Surface Energy Balance Modeling at Mountain Glaciers in Western Canada

The Cryosphere

Christina Draeger, Valentina Radić, Rachel H. White, and Mekdes Ayalew Tessema

Department of Earth Ocean and Atmospheric Sciences (EOAS),
The University of British Columbia, Vancouver, Canada

Correspondence: Christina Draeger (cdraeger@eoas.ubc.ca)

Supplementary Figures

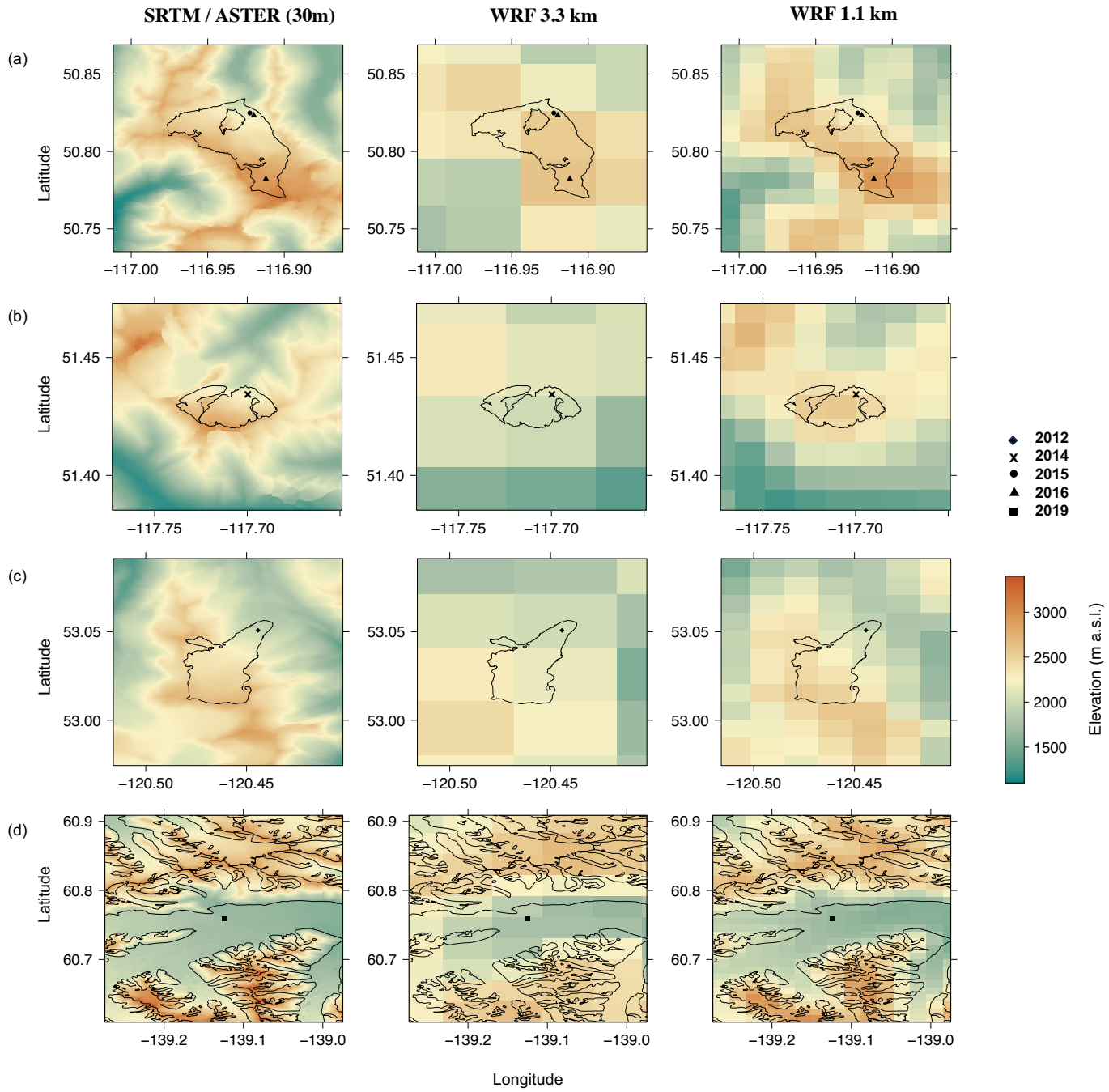

Figure S1: Topography for the domain covering (a) Conrad, (b) Nordic and (c) Castle Creek and (d) Kaskawulsh glaciers from a high-resolution DEM at 30 m grid spacing in comparison to the topography from WRF at 3.3 km and 1.1 km grid spacing. DEM data from SRTM (NASA JPL, 2013; Farr et al., 2007) were used for Castle Creek, Nordic and Conrad glaciers, and ASTER (ASTER, 2019; Abrams et al., 2020) for Kaskawulsh glacier. Markers indicate the AWS sites in different years. The outlines of the glaciers (black lines) are taken from the Randolph Glacier Inventory (RGI V6; RGI Consortium, 2017). Only on the map with Kaskawulsh glacier the neighboring glaciers are also shown.

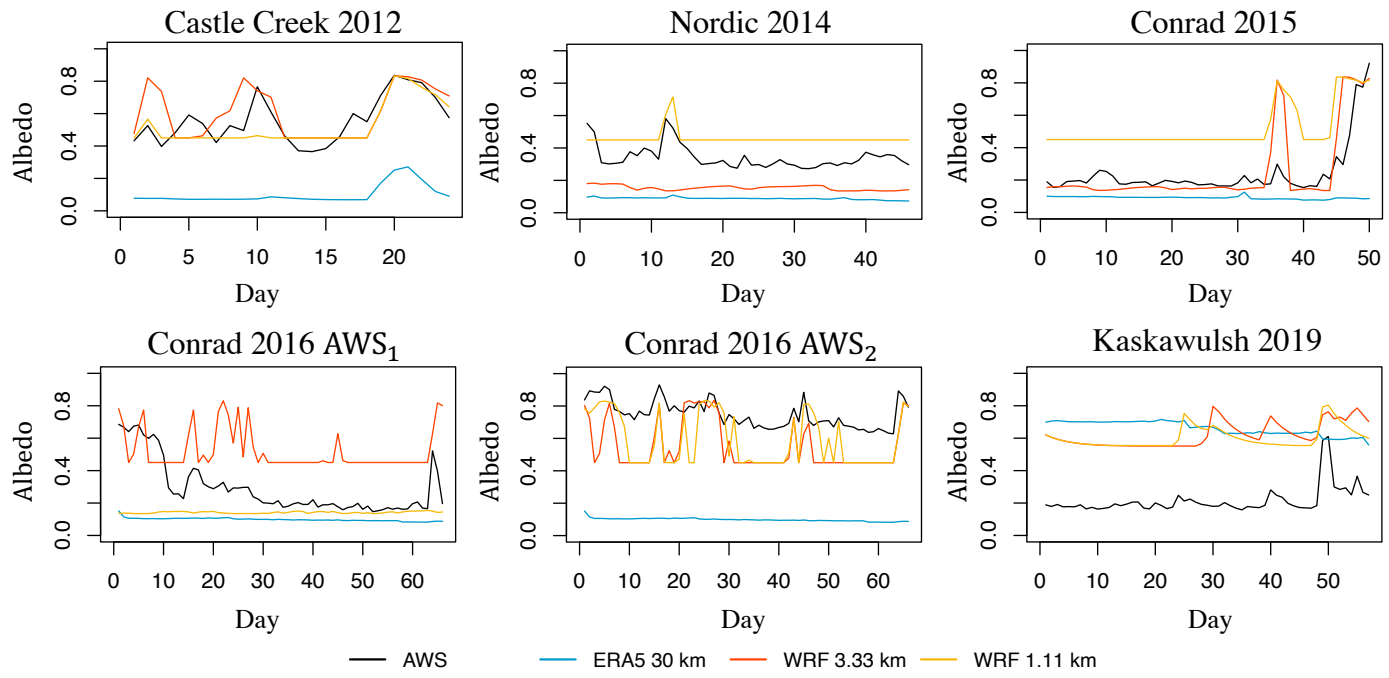

Figure S2: Modeled (ERA5, WRF at 3.3 km and WRF at 1.1 km) versus observed (AWS data) timeseries of daily albedo over the observational period. WRF is run with the REF configuration.

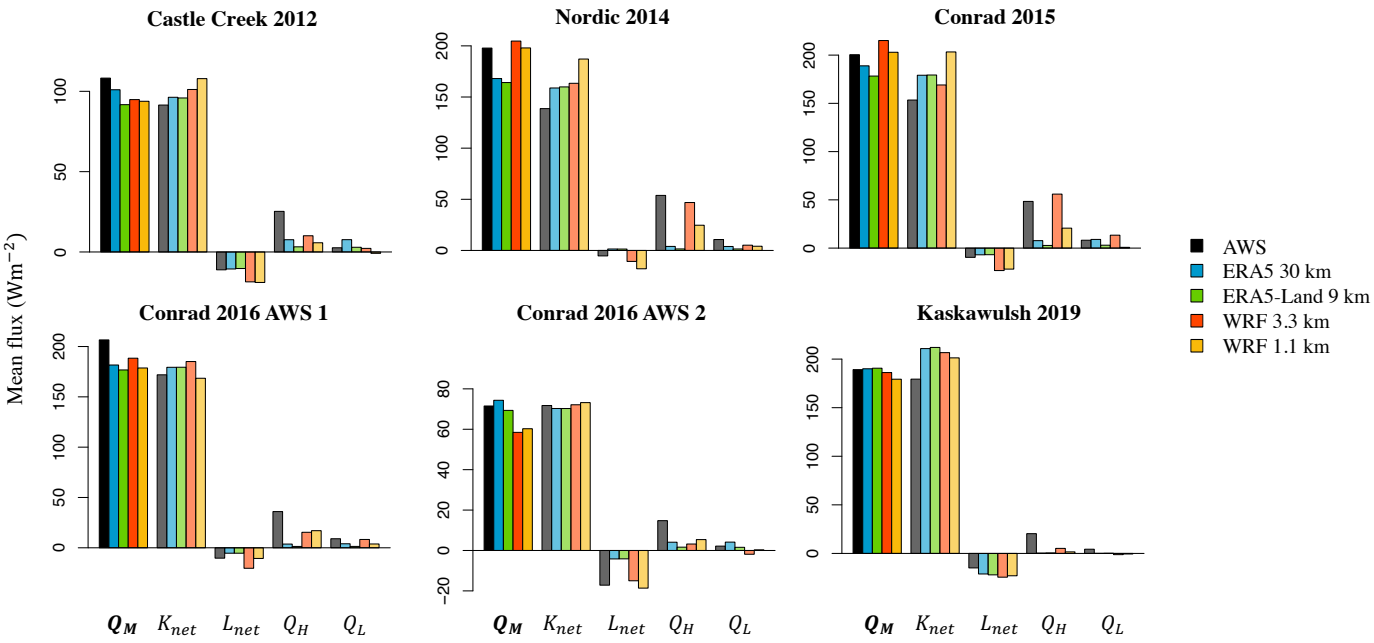

Figure S3: Mean daily total of melt energy (Q_M), as averaged over the observational period at each site, and the mean daily SEB components, including net shortwave (K_{net}) and longwave (L_{net}) radiation, sensible (Q_H) and latent (Q_L) heat fluxes, per glacier site calculated with different datasets (different colors). The REF configuration is used in the WRF runs. For this figure, only hourly values with $Q_M > 0$ are used in the calculation of mean daily fluxes.

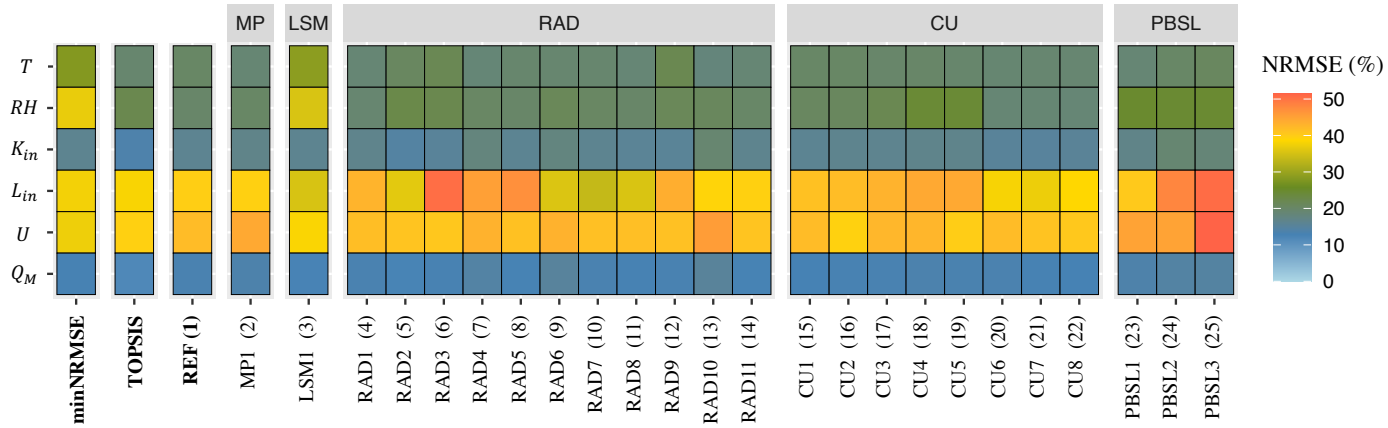

Figure S4: Visual representation of NRMSE calculated from the multiple 6-day WRF runs with three different configurations (minNRMSE, TOPSIS, REF) and the configurations used in the sensitivity runs (enumerated in brackets) with labels corresponding to their parameterization category with scheme that differs from REF. For full names of parameterization categories see Table S3. The NRMSE is calculated for each of the following variables: air temperature (T), relative humidity (RH), incoming shortwave (K_{in}) and longwave (L_{in}) radiation, wind speed (U) and total melt energy (Q_M).

Supplementary Tables

Table S1: Elevation for each study site (in meter above sea level) derived from AWS (on-site GPS), ERA5 at 30 km grid spacing, ERA5-Land at 9 km, WRF at 3.3 km and 1.1 km, and a high-resolution DEM at 30 m grid spacing: SRTM (NASA JPL, 2013; Farr et al., 2007) for Castle Creek, Nordic and Conrad glaciers, and ASTER (ASTER, 2019; Abrams et al., 2020) for Kaskawulsh glacier).

Glacier site	**AWS**	**ERA5**	**ERA5-Land**	**WRF 3.3 km**	**WRF 1.1 km**	**SRTM / ASTER**
Castle Creek 2012	1967	1762	1987	2157	1915	1977
Nordic 2014	2208	1785	1866	2124	2298	2203
Conrad 2015	2138	1901	2145	2412	2184	2163
Conrad 2016 AWS_1	2164	1901	2145	2567	2217	2182
Conrad 2016 AWS_2	2909	1901	2145	2618	2944	2910
Kaskawulsh 2019	1666	2122	2159	1709	1659	1709

Table S2: Summary of WRF configurations with physics parameterization schemes used in the 25 sensitivity runs. Radiation schemes (RAD) are split into longwave (LW) and shortwave (SW) schemes. The choice of planetary boundary (PBL) and surface layer (SL) schemes is interdependent, and therefore aggregated into one PBSL category. In the parameterization for the cumulus process (CU), the on/off label in brackets refers to the parameterization being switched 'on' or 'off' in each of the WRF domains d_1 (30 km) – d_2 (10 km) – d_3 (3.3 km) – d_4 (1.1 km). For each of the sensitivity runs, only one physics parameterization scheme is changed at a time, and all other specifications are the same as for the reference (REF) configuration (Tables 2 and S3).

Microphysics (MP)	
MP1	Morrison 2-Moment[1]
Land Surface Model (LSM)	
LSM1	Unified Noah[2]
Radiation (RAD)	
RAD1	LW/SW: CAM[3]
RAD2	LW: RRTM[4], SW: Dhudia [5]
RAD3	LW: CAM, SW: Dhudia
RAD4	LW: CAM, SW: Goddard[6]
RAD5	LW: CAM, SW: RRTMG[7]
RAD6	LW: RRTM, SW: Goddard
RAD7	LW: RRTM, SW: CAM
RAD8	LW: RRTM, SW: RRTMG
RAD9	LW: RRTMG. SW: Dhudia
RAD10	LW: RRTMG. SW: Goddard
RAD11	LW: RRTMG, SW: CAM

Cumulus (CU)	
CU1	Grell 3D Ensemble[8] (on – on – on – off)
CU2	Grell 3D Ensemble (on – on – on – on)
CU3	Kain–Fritsch[9] (on – on – off – off)
CU4	Kain–Fritsch (on – on – on – off)
CU5	Kain–Fritsch (on – on – on – on)
CU6	Betts–Miller–Janjic[10] (on – on – off – off)
CU7	Betts–Miller–Janjic (on – on – on – off)
CU8	Betts–Miller–Janjic (on – on – on – on)
Planetary Bound./Surface Layer (PBSL)	
PBSL1	PBL: MYNN[11] Level 2.5 SL: MYNN
PBSL2	PBL: Yonsei University[12] SL: Revised MM5[13]
PBSL3	PBL: Mellor–Yamada–Janjic (MYJ)[14] SL: Eta Similarity[15]

1 Morrison et al. (2009)
2 Tewari et al. (2004)
3 Collins et al. (2004)
4 Mlawer et al. (1997)
5 Dudhia (1989)
6 Max and Suarez (1994); Matsui et al. (2018)
7 Iacono et al. (2008)
8 Grell (1993); Grell and Dévényi (2002)
9 Kain (2004); The Kain-Fritsch trigger option was set to default.
10 Janjić (1994)
11 Nakanishi and Niino (2006, 2009); Olson et al. (2019)
12 Hong et al. (2006)
13 Jiménez et al. (2012)
14 Janjić (1994); Mesinger (1993)
15 Monin and Obukhov (1954); Janjić (1994, 1996, 2002)

Table S3: WRF physics parameterizations, for different physical processes, used in the three configurations: REF, minNRMSE and TOPSIS. In the parameterization for the cumulus process, the on/off label in brackets refers to the parameterization being switched 'on' or 'off' in each of the WRF domains d_1 (30 km) – d_2 (10 km) – d_3 (3.3 km) – d_4 (1.1 km).

Process	REF	minNRMSE	TOPSIS
Microphysics	Thompson[1]	Thompson	Thompson
Land Surface Model	Noah-MP	Unified Noah[2]	Noah-MP[3]
Longwave Radiation	RRTMG[5]	RRTM[4]	RRTM
Shortwave Radiation	RRTMG	Dhudia[6]	Dhudia
Cumulus	Grell 3D Ensemble[7] (on – on – on – off)	Grell 3D Ensemble (on – on – on – off)	Betts–Miller–Janjic[8] (on – on – on – on)
Planetary Boundary Layer	MYNN [9] Level 3	MYNN Level 3	MYNN Level 3
Surface Layer	MYNN	MYNN	MYNN

1 Thompson et al. (2008)
2 Tewari et al. (2004)
3 Niu et al. (2011); Yang et al. (2011)
4 Mlawer et al. (1997)
5 Iacono et al. (2008)
6 Dudhia (1989)
7 Grell (1993); Grell and Dévényi (2002)
8 Janjić (1994)
9 Nakanishi and Niino (2006, 2009); Olson et al. (2019)

Table S4: EC-derived roughness lengths (units in m) for momentum (z_{0v}), temperature (z_{0T}) and humidity (z_{0q}) used in the calculations of sensible and latent heat fluxes at each study site.

Site	z_{0v}	z_{0t}	z_{0q}
Castle Creek 2012	$10^{-2.5}$	$10^{-4.5}$	$10^{-4.0}$
Nordic 2014	$10^{-2.5}$	$10^{-5.0}$	$10^{-6.0}$
Conrad 2015	$10^{-2.5}$	$10^{-4.0}$	$10^{-3.5}$
Conrad 2016 AWS_1	$10^{-3.0}$	$10^{-4.5}$	$10^{-4.5}$
Conrad 2016 AWS_2	$10^{-2.5}$	$10^{-5.0}$	$10^{-5.0}$
Kaskawulsh 2019	$10^{-3.1}$	$10^{-5.9}$	$10^{-5.9}$

Table S5: Model performance, evaluated by r_{sp} and NNSE, over the whole observational period in simulating daily: air temperature (T), relative humidity (RH), wind speed (U), incoming shortwave (K_{in}) and longwave (L_{in}) radiation, sensible (Q_H) and latent (Q_L) heat fluxes and total melt energy (Q_M). The melt energy is estimated according to the SEB model (Eq. 1). The WRF runs are based on three configurations of physics parameterizations: REF, minNRMSE and TOPSIS. The model performance is shown as the mean (± one standard deviation) across the six study sites, with equal weighing of each site. Values in bold highlight the best performing model for the given variable. Values in purple highlight a statistically significant correlation at the 5 % confidence level for at least four of the six glacier sites.

Variable	**ERA5 30 km**	**ERA5-Land 9 km**	**WRF 3.3 km REF**	**WRF 3.3 km minNRMSE**	**WRF 3.3 km TOPSIS**	**WRF 1.1 km REF**	**WRF 1.1 km TOPSIS**	**WRF 1.1 km minNRMSE**
				r_{sp}				
T	0.86 ± 0.19	0.89 ± 0.14	0.89 ± 0.05	0.86 ± 0.04	0.88 ± 0.03	**0.91** ± 0.03	0.88 ± 0.03	0.90 ± 0.01
RH	0.74 ± 0.20	**0.75** ± 0.15	0.70 ± 0.21	0.55 ± 0.19	0.72 ± 0.19	0.71 ± 0.20	0.53 ± 0.25	0.71 ± 0.17
U	0.19 ± 0.36	0.13 ± 0.32	0.15 ± 0.15	0.10 ± 0.16	0.16 ± 0.20	**0.23** ± 0.20	0.20 ± 0.20	0.19 ± 0.24
K_{in}	**0.80** ± 0.09	**0.80** ± 0.09	0.60 ± 0.10	0.58 ± 0.19	0.56 ± 0.11	0.52 ± 0.16	0.55 ± 0.18	0.47 ± 0.14
L_{in}	**0.79** ± 0.11	0.78 ± 0.12	0.62 ± 0.07	0.56 ± 0.11	0.41 ± 0.12	0.54 ± 0.07	0.54 ± 0.14	0.35 ± 0.17
Q_H	0.29 ± 0.36	0.23 ± 0.38	0.54 ± 0.23	0.47 ± 0.23	**0.50** ± 0.24	0.47 ± 0.25	0.49 ± 0.33	0.40 ± 0.30
Q_L	0.20 ± 0.18	0.15 ± 0.22	0.55 ± 0.14	0.48 ± 0.19	0.55 ± 0.17	0.59 ± 0.12	0.53 ± 0.14	**0.61** ± 0.10
Q_M	**0.86** ± 0.05	**0.86** ± 0.04	0.72 ± 0.11	0.72 ± 0.10	0.69 ± 0.15	0.74 ± 0.10	0.73 ± 0.10	0.73 ± 0.12
				NNSE (%)				
T	58 ± 25	54 ± 24	56 ± 18	46 ± 11	55 ± 18	**62** ± 29	51 ± 11	**62** ± 29
RH	22 ± 10	24 ± 11	47 ± 24	30 ± 23	48 ± 23	**48** ± 24	38 ± 16	44 ± 23
U	17 ± 9	14 ± 6	27 ± 7	23 ± 9	**28** ± 9	24 ± 7	23 ± 10	23 ± 7
K_{in}	**69** ± 9	68 ± 10	49 ± 6	44 ± 20	49 ± 13	43 ± 4	45 ± 18	47 ± 10
L_{in}	**65** ± 13	**65** ± 14	41 ± 10	44 ± 10	39 ± 10	39 ± 10	45 ± 10	41 ± 11
Q_H	30 ± 12	27 ± 9	39 ± 10	33 ± 9	**41** ± 10	38 ± 11	33 ± 10	37 ± 10
Q_L	42 ± 8	45 ± 10	44 ± 7	47 ± 8	41 ± 4	**50** ± 7	**50** ± 7	47 ± 5
Q_M	**78** ± 10	75 ± 9	63 ± 9	53 ± 10	56 ± 6	69 ± 6	54± 12	60 ± 7

Table S6: Model performance, evaluated by MAPE and NMBE, over the whole observational period in simulating daily: air temperature (T), relative humidity (RH), wind speed (U), incoming shortwave (K_{in}) and longwave (L_{in}) radiation, sensible (Q_H) and latent (Q_L) heat fluxes and total melt energy (Q_M). The melt energy is estimated according to the SEB model (Eq. 1). The WRF runs are based on three configurations of physics parameterizations: REF, minNRMSE and TOPSIS. The model performance is shown as the mean (± one standard deviation) across the six study sites, with equal weighing of each site. Values in bold highlight the best performing model for the given variable.

Variable	**ERA5 30 km**	**ERA5-Land 9 km**	**WRF 3.3 km**			**WRF 1.1 km**		
			REF	**minNRMSE**	**TOPSIS**	**REF**	**minNRMSE**	**TOPSIS**
MAPE (%)								
T	67 ± 60	71 ± 52	57 ± 43	67 ± 47	**54** ± 36	63 ± 53	71 ± 53	53 ± 34
RH	33 ± 14	31 ± 13	16 ± 5	27 ± 12	16 ± 7	**15** ± 5	20 ± 8	17 ± 6
U	61 ± 10	71 ± 7	43 ± 7	48± 9	**41** ± 7	46 ± 13	49 ± 14	46 ± 11
K_{in}	**23** ± 7	**23** ± 7	37 ± 7	32 ± 7	29 ± 4	41 ± 17	31 ± 4	32 ± 7
L_{in}	**4** ± 2	**4** ± 3	7 ± 1	6 ± 2	7 ± 1	7 ± 2	6 ± 1	7 ± 1
Q_H	94 ± 22	98 ± 18	89 ± 28	99 ± 31	87 ± 29	81 ± 23	101 ± 30	**78** ± 25
Q_L	279 ± 227	**150** ± 76	268 ± 150	284 ± 185	255 ± 115	234 ± 191	263 ± 157	215 ± 155
Q_M	**18** ± 3	**18** ± 2	25 ± 4	32 ± 10	30 ± 4	23 ± 3	31 ± 9	27 ± 5
NMBE (%)								
T	-9 ± 73	2 ± 69	-13 ± 42	-33 ± 50	**0** ± 46	-17 ± 48	-43 ± 43	-2 ± 37
RH	33 ± 14	31 ± 13	**-3** ± 14	19 ± 23	-6 ± 13	-9± 11	11± 17	-12 ± 9
U	-61 ± 10	-71 ± 7	-20 ± 18	-36 ± 14	**-16** ± 20	-40 ± 16	-42 ± 13	-38 ± 15
K_{in}	18 ± 10	18 ± 10	20 ± 10	-14 ± 19	**0** ± 11	31 ± 24	-7 ± 21	9 ± 14
L_{in}	**0** ± 4	**0** ± 4	-5 ± 3	**0** ± 4	-2 ± 3	-5 ± 3	-1 ± 3	-2 ± 2
Q_H	-86 ± 32	-96 ± 19	-36 ± 28	-68 ± 13	**-17** ± 28	-59 ± 27	-77 ± 14	-44 ± 23
Q_L	-194 ± 237	-126 ± 78	41 ± 150	-70 ± 83	**2** ± 140	5 ± 195	-5 ± 137	-24 ± 151
Q_M	**1** ± 8	-4 ± 8	-2 ± 11	-27 ± 13	-14 ± 18	-3 ± 10	-25 ± 13	-15 ± 10

Supplementary References

Abrams, M., Crippen, R., and Fujisada, H. (2020). ASTER Global Digital Elevation Model (GDEM) and ASTER Global Water Body Dataset (ASTWBD). *Remote Sensing*, 12(7).

Collins, W., Rasch, P., Boville, B., Hack, J., Mccaa, J., Williamson, D., and Kiehl, J. (2004). Description of the NCAR community atmosphere model (CAM 3.0). *NCAR Technical Note*, TN-464+STR.

Dudhia, J. (1989). Numerical study of convection observed during the Winter Monsoon Experiment using a mesoscale two-dimensional model. *Journal of The Atmospheric Sciences*, 46:3077–3107.

Farr, T. G., Rosen, P. A., Caro, E., Crippen, R., Duren, R., Hensley, S., Kobrick, M., Paller, M., Rodriguez, E., Roth, L., Seal, D., Shaffer, S., Shimada, J., Umland, J., Werner, M., Oskin, M., Burbank, D., and Alsdorf, D. (2007). The Shuttle Radar Topography Mission. *Reviews of Geophysics*, 45(2).

Grell, G. A. (1993). Prognostic evaluation of assumptions used by cumulus parameterizations. *Monthly Weather Review*, 121(3):764 – 787.

Grell, G. A. and Dévényi, D. (2002). A generalized approach to parameterizing convection combining ensemble and data assimilation techniques. *Geophysical Research Letters*, 29(14):38–1–38–4.

Hong, S.-Y., Noh, Y., and Dudhia, J. (2006). A new vertical diffusion package with an explicit treatment of entrainment processes. *Monthly Weather Review*, 134(9):2318 – 2341.

Iacono, M. J., Delamere, J. S., Mlawer, E. J., Shephard, M. W., Clough, S. A., and Collins, W. D. (2008). Radiative forcing by long-lived greenhouse gases: Calculations with the AER radiative transfer models. *Journal of Geophysical Research: Atmospheres*, 113(D13).

Janjić, Z. I. (1994). The step-mountain eta coordinate model: Further developments of the convection, viscous sublayer, and turbulence closure schemes. *Monthly Weather Review*, 122(5):927 – 945.

Janjić, Z. I. (1996). The surface layer in the NCEP eta model. In *Eleventh Conference on Numerical Weather Prediction, Norfolk, VA, 19-23 August, Amererican Meteor Society, Boston, MA*, pages 345–355.

Janjić, Z. I. (2002). Nonsingular implementation of the Mellor–Yamada Level 2.5 scheme in the NCEP meso model. *NCEP Office Note*, 436.

Jiménez, P. A., Dudhia, J., González-Rouco, J. F., Navarro, J., Montávez, J. P., and García-Bustamante, E. (2012). A revised scheme for the WRF surface layer formulation. *Monthly Weather Review*, 140(3):898 – 918.

Kain, J. S. (2004). The Kain-Fritsch convective parameterization: An update. *Journal of Applied Meteorology*, 43(1):170 – 181.

Matsui, T., Zhang, S. Q., Lang, S. E., Tao, W.-K., Ichoku, C., and Peters-Lidard, C. D. (2018). Impact of radiation frequency, precipitation radiative forcing, and radiation column aggregation on convection-permitting West African monsoon simulations. *Climate Dynamics*, 55(1-2):193–213.

Max, M.-D. C. and Suarez, M. J. (1994). An efficient thermal infrared radiation parameterization for use in general circulation models. *NASA Technical Memorandum*, 3(104606):85.

Mesinger, F. (1993). Forecasting upper tropospheric turbulence within the framework of the Mellor-Yamada 2.5 closure. In *Res. Activ. in Atmos. and Ocean. Mod., WMO, Geneva, CAS/JSC WGNE*, volume 18, pages 4.28–4.29.

Mlawer, E. J., Taubman, S. J., Brown, P. D., Iacono, M. J., and Clough, S. A. (1997). Radiative transfer for inhomogeneous atmospheres: RRTM, a validated correlated-k model for the longwave. *Journal of Geophysical Research: Atmospheres*, 102(D14):16663–16682.

Monin, A. S. and Obukhov, A. M. (1954). Basic laws of turbulent mixing in the surface layer of the atmosphere. *Contrib. Geophys. Inst. Acad. Sci. USSR*, 24:163–187.

Morrison, H., Thompson, G., and Tatarskii, V. (2009). Impact of cloud microphysics on the development of trailing stratiform precipitation in a simulated squall line: Comparison of one- and two-moment schemes. *Monthly Weather Review*, 137(3):991 – 1007.

Nakanishi, M. and Niino, H. (2006). An improved Mellor–Yamada Level-3 model: Its numerical stability and application to a regional prediction of advection fog. *Boundary-Layer Meteorology*, 119:397–407.

Nakanishi, M. and Niino, H. (2009). Development of an improved turbulence closure model for the atmospheric boundary layer. *Journal of the Meteorological Society of Japan. Ser. II*, 87(5):895–912.

NASA Jet Propulsion Laboratory (JPL (2013). Shuttle Radar Topography Mission (SRTM) 1 Arc-Second Global [Data set]. NASA Earth Data. Accessed on August 1, 2020.

NASA/METI/AIST/Japan Spacesystems and U.S./Japan ASTER Science Team (2019). ASTER Global Digital Elevation Model V003 [Data set]. NASA EOSDIS Land Processes DAAC. Accessed on August 1, 2020.

Niu, G.-Y., Yang, Z.-L., Mitchell, K. E., Chen, F., Ek, M. B., Barlage, M., Kumar, A., Manning, K., Niyogi, D., Rosero, E., Tewari, M., and Xia, Y. (2011). The community Noah land surface model with multiparameterization options (Noah-MP): 1. Model description and evaluation with local-scale measurements. *Journal of Geophysical Research: Atmospheres*, 116(D12).

Olson, J. B., Kenyon, J. S., Angevine, W. A., Brown, J. M., and Pagowski, Mariusz abd Sušelj, K. (2019). A description of the MYNN-EDMF Scheme and the coupling to other components in WRF–ARW. *OAA Technical Memorandum OAR GSD*, 61:37.

RGI Consortium (2017). Randolph glacier inventory – A dataset of global glacier outlines, version 6. NSIDC: National Snow and Ice Data Center. Accessed on May 01, 2022.

Tewari, M., Chen, F., Wang, W., Dudhia, J., Lemone, A., Mitchell, E., Ek, M., Gayno, G., Wegiel, W., and Cuenca, R. H. (2004). Implementation and verification of the united N land surface model in the WRF model. In *20th Conference on Weather Analysis and Forecasting/16th Conference on Numerical Weather Prediction*, pages 11–15.

Thompson, G., Field, P., Rasmussen, R., and Hall, W. (2008). Explicit forecasts of winter precipitation using an improved bulk microphysics scheme. Part II: Implementation of a new snow parameterization. *Monthly Weather Review*, 136:5095 – 5115.

Yang, Z.-L., Niu, G.-Y., Mitchell, K. E., Chen, F., Ek, M. B., Barlage, M., Longuevergne, L., Manning, K., Niyogi, D., Tewari, M., and Xia, Y. (2011). The community Noah land surface model with multiparameterization options (Noah-MP): 2. Evaluation over global river basins. *Journal of Geophysical Research: Atmospheres*, 116(D12).